Journal of Biomechanics 49 (2016) 1554–1561

Contents lists available at ScienceDirect

Journal of Biomechanics

journal homepage: www.elsevier.com/locate/jbiomech
www.JBiomech.com

The influence of wheelchair propulsion hand pattern on upper extremity muscle power and stress

Jonathan S. Slowik [a], Philip S. Requejo [b,c], Sara J. Mulroy [b], Richard R. Neptune [a,*]

[a] Department of Mechanical Engineering, The University of Texas at Austin, Austin, TX, USA
[b] Pathokinesiology Laboratory, Rancho Los Amigos National Rehabilitation Center, Downey, CA, USA
[c] Rehabilitation Engineering, Rancho Los Amigos National Rehabilitation Center, Downey, CA, USA

ARTICLE INFO

Article history:
Accepted 18 March 2016

Keywords:
Forward dynamics simulation
Musculoskeletal model
Propulsion pattern
Biomechanics

ABSTRACT

The hand pattern (i.e., full-cycle hand path) used during manual wheelchair propulsion is frequently classified as one of four distinct hand pattern types: arc, single loop, double loop or semicircular. Current clinical guidelines recommend the use of the semicircular pattern, which is based on advantageous levels of broad biomechanical metrics implicitly related to the demand placed on the upper extremity (e.g., lower cadence). However, an understanding of the influence of hand pattern on specific measures of upper extremity muscle demand (e.g., muscle power and stress) is needed to help make such recommendations, but these quantities are difficult and impractical to measure experimentally. The purpose of this study was to use musculoskeletal modeling and forward dynamics simulations to investigate the influence of the hand pattern used on specific measures of upper extremity muscle demand. The simulation results suggest that the double loop and semicircular patterns produce the most favorable levels of overall muscle stress and total muscle power. The double loop pattern had the lowest full-cycle and recovery-phase upper extremity demand but required high levels of muscle power during the relatively short contact phase. The semicircular pattern had the second-lowest full-cycle levels of overall muscle stress and total muscle power, and demand was more evenly distributed between the contact and recovery phases. These results suggest that in order to decrease upper extremity demand, manual wheelchair users should consider using either the double loop or semicircular pattern when propelling their wheelchairs at a self-selected speed on level ground.

1. Introduction

The manual wheelchair propulsion cycle can be divided into the contact phase, when mechanical power is delivered to the wheelchair via hand contact with the handrim, and the recovery phase, when the hand is repositioned in preparation for the next cycle (e.g., Kwarciak et al., 2009). During the contact phase, the hand is constrained to the arc of the handrim. However, during the recovery phase, the hand is much less constrained and can follow a number of different paths. The resulting hand patterns (i.e., full-cycle hand paths) are frequently classified into four distinct hand pattern types based on the shape of their projection onto the plane of the handrim: arc (*AR*), single loop (*SL*), double loop (*DL*) and semicircular (*SC*) (Fig. 1, e.g., Boninger et al., 2002). The hand pattern is a clinically visible indicator that can provide insight into an individual's propulsion technique due to the close relationship between the movement of the hand and propulsion mechanics (e.g., Shimada et al., 1998).

Previous investigations have attempted to determine whether the choice of hand pattern influences the likelihood of developing upper extremity pain and injury (e.g., Boninger et al., 2002; de Groot et al., 2004; Kwarciak et al., 2012; Qi et al., 2014). Most of these studies have focused on the influence of hand pattern on broad biomechanical metrics that have been identified as risk factors (e.g., cadence, peak handrim force). Results suggest that *SC* produces lower cadence, larger contact percentages, larger contact angles, longer push distances and lower peak forces (e.g., Boninger et al., 2002; Kwarciak et al., 2012; Qi et al., 2014). *SC* also produces lower joint accelerations (Shimada et al., 1998) and results in a clearer separation between contact and recovery muscle activity timing (Qi et al., 2014). As a result, current clinical guidelines recommend the use of *SC*, citing many potentially advantageous levels of these biomechanical metrics (PVACSCM, 2005).

However, other hand patterns may also have favorable characteristics. Kwarciak et al. (2012) found that *DL* is associated with

* Corresponding author. Tel.: +512 471 0848; fax: +512 471 8727.
E-mail address: rneptune@mail.utexas.edu (R.R. Neptune).

http://dx.doi.org/10.1016/j.jbiomech.2016.03.031
0021-9290/

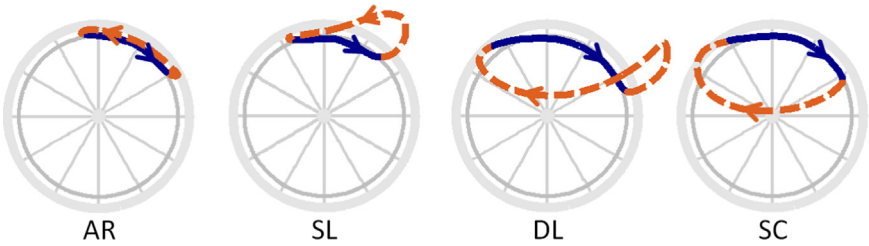

Fig. 1. Hand pattern definitions. The four hand pattern types are arc (*AR*), single loop (*SL*), double loop (*DL*) and semicircular (*SC*). The solid line denotes the contact phase, while the dashed line denotes the recovery phase. The arrows indicate the direction of hand motion and the direction of wheelchair propulsion is to the right.

an increased contact angle, decreased cadence and decreased braking moment, leading them to recommend its use. *DL* and *AR* have also been shown to have the lowest integrated electromyography (iEMG) values among the hand patterns (Kwarciak et al., 2012). Others have found that *AR* is a more metabolically efficient hand pattern than *SC* (de Groot et al., 2004).

While previous investigations of hand pattern differences have been largely focused on broad biomechanical metrics that have been related to upper extremity demand (e.g., cadence, contact angle), a detailed investigation of how specific measures of upper extremity demand such as muscle power and stress vary across hand patterns could serve to further refine clinical propulsion technique training aimed at mitigating the negative consequences of increased shoulder loads during manual wheelchair propulsion.

Forward dynamics modeling and simulation techniques provide a powerful framework for examining the biomechanics of a task at the individual muscle level (e.g., Erdemir et al., 2007) and allow the quantification of the upper extremity demand placed on individual muscles. The purpose of this study was to use musculoskeletal modeling and forward dynamics simulations to examine the influence of the four common hand pattern types on specific measures of upper extremity muscle demand (i.e., individual muscle power and stress). Based on the previously reported biomechanical advantages (e.g., low handrim forces, low cadence, large contact angle, and large contact percentage), we expected that overall the *SC* simulation would also have the lowest muscle demand. These results will help provide rationale for designing propulsion training programs aimed at reducing upper extremity demand and development of overuse injuries and pain in manual wheelchair users.

2. Methods

2.1. Musculoskeletal model

An upper extremity musculoskeletal model and dynamic optimization framework that have been previously described in detail (e.g., Rankin et al., 2010, 2011) were used in this study to generate forward dynamics simulations of manual wheelchair propulsion. The musculoskeletal model was based on the work of Holzbaur et al. (2005) and developed using SIMM (Musculographics, Inc., Santa Rosa, CA, USA). The model had six rotational degrees-of-freedom and included segments representing the trunk and right upper arm, forearm and hand. In addition to trunk lean, elbow flexion–extension and forearm pronation–supination, there were three degrees-of-freedom at the shoulder: plane-of-elevation, elevation angle and internal–external rotation (thoracohumeral angles). Scapulohumeral rhythm was defined using regression equations based on cadaver data (de Groot and Brand, 2001). Full-cycle trunk lean and contact-phase hand translations were prescribed based on experimentally-collected kinematic data. The dynamic equations-of-motion were generated using SD/FAST (Parametric Technology Corp., Needham, MA, USA). The major upper extremity muscles crossing the shoulder and elbow joints were represented by 26 Hill-type musculotendon actuators (see Slowik and Neptune, 2013) and governed by intrinsic muscle force–length–velocity and tendon force–strain relationships. Each actuator received a distinct excitation signal except the three latissimus dorsi actuators, the two sternocostal pectoralis major actuators, and the two actuators representing the lateral triceps and anconeus. Muscles within each of these groups received the same excitation signal. Muscle excitation–activation dynamics were modeled using a first order differential equation (Raasch et al., 1997) with muscle-specific activation and deactivation time constants (Happee and van der Helm, 1995; Winters and Stark, 1988). The musculotendon lengths and moment arms were determined using polynomial regression equations (Rankin and Neptune, 2012), and the product of each muscle moment arm and force was applied at the joint as a muscle moment. Passive torques were applied at the joints to represent ligaments and other passive joint structures that limit extreme joint positions (Davy and Audu, 1987).

2.2. Simulation and optimization framework

Each muscle excitation pattern was generated using a bimodal pattern defined by six parameters (e.g., Hall et al., 2011), resulting in a total of 132 optimization parameters. For each hand pattern type, the excitation parameters that produced a simulation that best emulated hand pattern subgroup-averaged experimental propulsion data (i.e., joint angle and 3D handrim force profiles; see *Experimental data* below) were identified using a simulated annealing optimization algorithm (Goffe et al., 1994) and an optimal tracking cost function (Neptune et al., 2001). To prevent excess co-contraction, an additional term was included in the cost function that minimized the muscle stress squared. Average power delivered to the handrim was kept constant (6 W) across simulations to allow for direct comparisons.

2.3. Experimental data

Experimental data was previously collected from 223 individuals with complete motor paraplegia while they propelled their wheelchair at a self-selected speed on a stationary ergometer that simulated level propulsion over a tile surface (e.g., Soltau et al., 2015). The subjects were recruited from outpatient clinics throughout the Rancho Los Amigos National Rehabilitation Center, and informed written consent was obtained in accordance with the governing Institutional Review Board. Further subject enrollment and inclusion criteria details are described elsewhere (Mulroy et al., 2015). The biomechanical data collection and processing procedures will be described briefly here. Subjects were allowed to acclimate until they felt comfortable, and then a ten-second trial was recorded following at least 30 s of propulsion to ensure near steady-state propulsion. Trunk, right side upper extremity and wheel kinematics were collected using a 4-scanner CODA motion analysis system (Charnwood Dynamics Ltd., Leicestershire, UK) with 15 active markers placed on landmarks on the body and right wheel (e.g., Lighthall-Haubert et al., 2009). Three-dimensional handrim kinetics were measured using an instrumented wheel (SmartWheel; Three Rivers Holdings, Mesa, AZ, USA).

Kinematic and kinetic data were low-pass filtered using a fourth-order zero-lag Butterworth filter with cutoff frequencies of 8 Hz and 10 Hz, respectively, in Visual3D (C-Motion, Inc., Germantown, MD, USA). Contact and recovery phases were delineated using a resultant handrim force threshold of 5 N. Contact and recovery-phase data for each cycle were time-normalized and averaged across propulsion cycles within each subject. A previously-described method (Rao et al., 1996) was used to locate the third metacarpophalangeal joint center (MCP3), and the hand pattern was defined as the average MCP3 path projected onto the plane of the handrim (e.g., Fig. 1). Hand patterns were characterized using a set of objective, quantitative parameters (see Slowik et al., 2015 for details), and this characterization was used to identify four groups of subjects that used each of the four hand pattern types. From these groups, twenty male subjects (five of each hand pattern type) were then identified such that differences between pattern-type group averages for age, time from injury, height, mass, body mass index and propulsion speed were minimized (Table 1). Mean subject data were then averaged across subjects within each pattern type group to create group-averaged hand pattern, joint angle and 3D handrim force profiles.

2.4. Analysis

Three consecutive propulsion cycles were simulated for each hand pattern type, and the third cycle was analyzed to allow the simulation to reach steady-state. To assess how well each simulation tracked the experimental data, root-mean-square (RMS) differences between the simulated and experimental data were calculated. Individual muscle data at each time step were then obtained from

Table 1
Mean values of subject and propulsion characteristics for the four hand pattern types: arc (*AR*), single loop (*SL*), double loop (*DL*) and semicircular (*SC*).

Subject characteristics						Propulsion characteristics			
Hand pattern type	Age (yr)	Time from injury (yr)	Height (m)	Mass (kg)	Body mass index (kg/m^2)	Propulsion speed (m/s)	Cycle time (s)	Contact percentage (%)	Contact angle (°)
AR	39.4	9.3	1.77	77.3	24.97	0.97	0.95	45.8	73.2
SL	39.2	14.2	1.80	77.6	23.98	1.02	1.02	36.4	71.7
DL	32.7	12.9	1.73	81.1	26.86	0.97	1.43	34.7	86.6
SC	35.0	10.0	1.77	79.9	25.35	0.99	1.34	44.9	92.9
All 20 subjects	36.6	11.6	1.77	79.0	25.29	0.99	1.19	40.5	81.1

the simulations and used to calculate specific measures of upper extremity muscle demand. Instantaneous muscle stress was calculated by dividing the instantaneous muscle force by the physiological cross-sectional area of the muscle, and time-averaged within the contact and recovery phases as well as across the full cycle. The full-cycle values were also decomposed into contributions during the contact and recovery phases, which enable additional comparisons across simulations that account for the differences in contact percentages.

Instantaneous muscle mechanical power was computed as the product of the instantaneous muscle force and velocity. Mean positive and negative power for the contact phase, recovery phase and full cycle were calculated by time-averaging the instantaneous positive and negative power, respectively. Mean total (absolute value sum) and net (linear sum) power were subsequently calculated. The full-cycle values were again decomposed into contributions from the contact and recovery phases. The individual muscle data from the 26 muscles were combined into 13 analysis groups based on a combination of anatomical location and muscle function (Table 2), with power data summed and stress data averaged within each muscle group. Overall measures of upper extremity demand were then calculated as the summed power and average stress of all 26 muscles.

Table 2
Upper extremity muscle and group definitions.

Muscle group	Muscle	Compartment	Abbreviation
ADelt	Deltoid	Anterior	DELT1
MDelt	Deltoid	Middle	DELT2
PDelt	Deltoid	Posterior	DELT3
Subsc	Subscapularis	–	SUBSC
Supra	Supraspinatus	–	SUPSP
Infra	Infraspinatus	–	INFSP
	Teres minor	–	TMIN
PecMaj	Pectoralis major	Clavicular head	PECM1
		Sternocostal head - sternum	PECM2
		Sternocostal head - ribs	PECM3
	Coracobrachialis	–	CORB
Lat	Latissimus dorsi	Thoracic	LAT1
		Lumbar	LAT2
		Iliac	LAT3
	Teres major	–	TMAJ
Tri	Triceps brachii	Long head	TRIlong
		Medial head	TRImed
		Lateral head	TRIlat
	Anconeus	–	ANC
Bra	Brachialis	–	BRA
	Brachioradialis	–	BRD
Bic	Biceps brachii	Long head	BIClong
		Short head	BICshort
Sup	Supinator	–	SUP
Pro	Pronator teres	–	PT
	Pronator quadratus	–	PQ

3. Results

3.1. Experimental data tracking

All four simulations resulted in propulsion mechanics that closely emulated the corresponding hand pattern type experimental joint kinematics and handrim forces (Table 3), with average RMS differences of 2.1° and 1.7 N, respectively. All RMS differences were well within one standard deviation of the experimental data.

3.2. Overall muscle power

Full-cycle net muscle power was similar across hand pattern types, with the lowest power generated with *SC* and the highest power generated with *SL* (7.0 W vs. 7.6 W, Fig. 2). While contact-phase net muscle power was larger for *SL* and *DL* compared to *AR* and *SC* (14.6 W and 15.2 W vs. 11.4 W and 11.3 W, respectively), contact-phase contributions to the full-cycle net muscle power were similar across all hand pattern types (range: 5.1–5.3 W). There were larger differences in the total muscle power, with *DL* requiring the least full-cycle total power and *AR* requiring the most (22.5 W vs. 26.5 W). The contact and recovery phases had comparable amounts of negative (eccentric) muscle power. However, the contact phase consistently had greater amounts of positive (concentric) muscle power than the recovery phase. As a result, the contact phase also had consistently larger total and net muscle power than the recovery phase, although the net power was positive during both phases for all hand pattern types. While the

Table 3
Root-mean-square differences between simulated and experimental joint kinematics and handrim forces for the four hand pattern types: arc (*AR*), single loop (*SL*), double loop (*DL*) and semicircular (*SC*). For comparison, one standard deviation of the experimental data is provided in parentheses to indicate inter-subject variability.

Tracking differences (simulation vs. experimental)		Simulations							
		AR		*SL*		*DL*		*SC*	
Joint kinematics (degrees)	Elevation plane	1.2	(10.3)	1.8	(19.1)	2.3	(13.3)	3.3	(12.4)
	Elevation angle	0.7	(5.3)	1.0	(7.3)	0.9	(6.4)	1.1	(8.2)
	Shoulder rotation	1.0	(23.6)	2.9	(32.4)	2.3	(18.0)	9.2	(26.0)
	Elbow flexion	0.9	(18.5)	0.7	(8.4)	0.8	(8.6)	0.8	(12.9)
	Pronation/supination	4.2	(23.6)	1.7	(12.0)	1.2	(11.6)	4.3	(22.5)
	All joints	1.6	(16.3)	1.6	(15.8)	1.5	(11.6)	3.7	(16.4)
Handrim forces (N)	Tangential	0.9	(5.2)	3.2	(3.8)	1.0	(6.2)	2.3	(5.5)
	Radial	3.3	(11.4)	0.8	(5.8)	1.9	(4.8)	2.0	(10.1)
	Lateral	0.7	(5.0)	1.7	(3.0)	1.7	(3.8)	1.3	(4.1)
	All forces	1.6	(7.2)	1.9	(4.2)	1.5	(4.9)	1.9	(6.6)

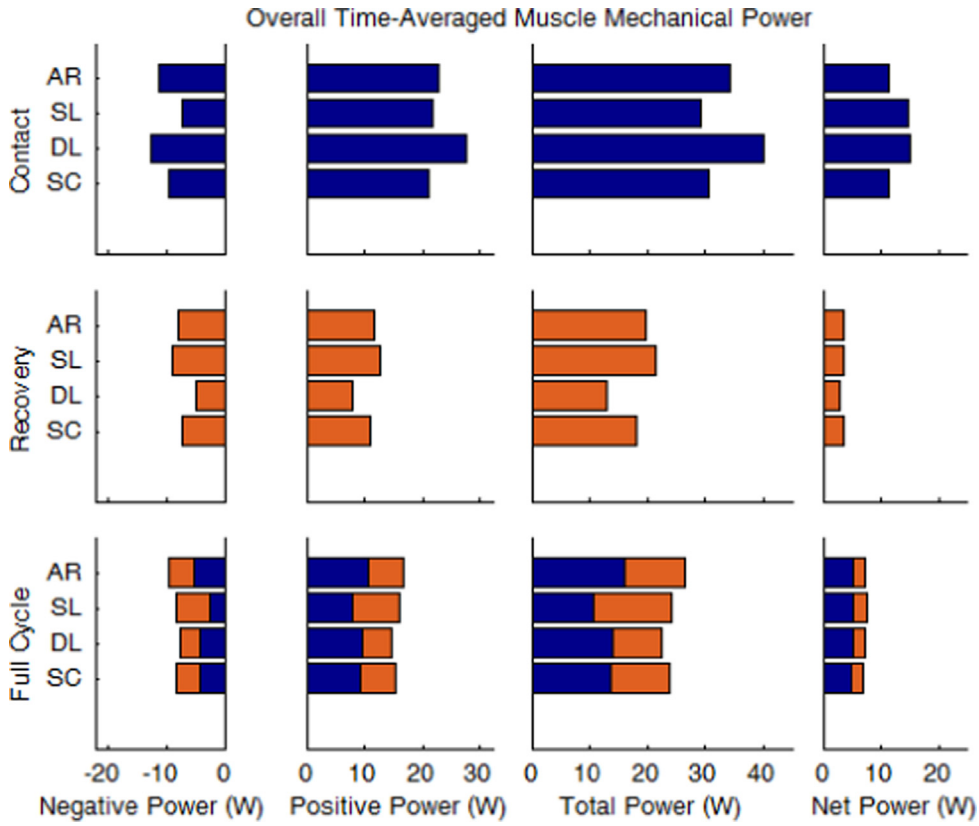

Fig. 2. Overall levels of time-averaged negative, positive, total and net power (summed across all muscles) for the four hand pattern types: arc (*AR*), single loop (*SL*), double loop (*DL*) and semicircular (*SC*). The top, middle and bottom rows correspond to the contact phase, recovery phase and full cycle, respectively. Contact and recovery-phase contributions are indicated with darker (blue) and lighter (orange) shading, respectively.

recovery-phase contributions accounted for only a small portion of the full-cycle net power (26–30%), recovery-phase power accounted for a much larger portion of the full-cycle total power (37–57%).

3.3. Individual muscle power

For all hand pattern types, ADelt and Tri were among the primary contributors to the full-cycle total and net muscle power (Fig. 3). The majority of this power was generated during the contact phase. Other large contributors to the full-cycle total muscle power included PDelt, Lat and Bra with *AR*; MDelt and Bra with *SL*; and Lat with *SC*.

Comparisons between hand pattern types revealed a few differences in individual muscle power generation. Full-cycle Lat total power generation was increased with *AR*. Full-cycle MDelt total power generation was increased with *SL*, but full-cycle ADelt total power generation was decreased. Contact-phase ADelt and Tri total power generation was increased with *DL*, but contact-phase PecMaj and recovery-phase Lat total power generation was decreased. Total power generation was not notably higher or lower for any individual muscle group with *SC* relative to the other hand pattern types.

3.4. Overall muscle stress

Full-cycle muscle stress was lowest with *DL* and highest with *AR* (31.5 kPa vs. 43.0 kPa, Fig. 4). Contact-phase stress was lowest with *SC* and highest with *SL* (39.4 kPa vs. 50.7 kPa). However, contact-phase contribution to the full-cycle muscle stress was lowest with *DL* and highest with *AR* (14.7 kPa vs. 22.6 kPa). Recovery-phase stress was lowest with *DL* and highest with *AR* (25.8 kPa vs. 38.0 kPa). While recovery-phase contribution to the full-cycle muscle stress was also lowest with *DL*, it was highest with *SL* (16.8 kPa vs. 21.9 kPa). Recovery-phase muscle stress was consistently lower than contact-phase muscle stress, with percent differences between contact and recovery values ranging from 5% (*SC*) to 48% (*DL*). However, the recovery phase consistently contributed approximately half of the full-cycle muscle stress (46–53%) due to the longer duration of this phase.

3.5. Individual muscle stress

For all hand pattern types, Subsc, MDelt, PDelt and ADelt were among the muscle groups that experienced the highest full-cycle stress levels (Fig. 5). The majority of the full-cycle ADelt stress was attributed to high stress during the contact phase, while the majority of the full-cycle PDelt and Subsc stresses were attributed to the high stresses during the recovery phase. The high full-cycle MDelt stress was attributed to high stresses during both phases. Other high full-cycle muscle stress values occurred in Lat and Sup with *AR*; Infra, Bra, Pro and Sup with *SL*; and Bra and Sup with *SC*.

Comparisons between hand pattern types revealed a number of differences in individual muscle stress levels. *AR* experienced relatively high full-cycle MDelt stress due to contributions during both phases. *AR* also experienced high contact-phase stress from Sup and high recovery-phase stress from Lat. However, *AR* experienced low full-cycle stress from Subsc compared to other hand pattern types, primarily due to low stress during the recovery phase. *SL* experienced high full-cycle Infra stress, primarily due to the high stress during the contact phase. *SL* also experienced high full-cycle Subsc stress, due to high stress during the recovery phase. In addition, *SL*

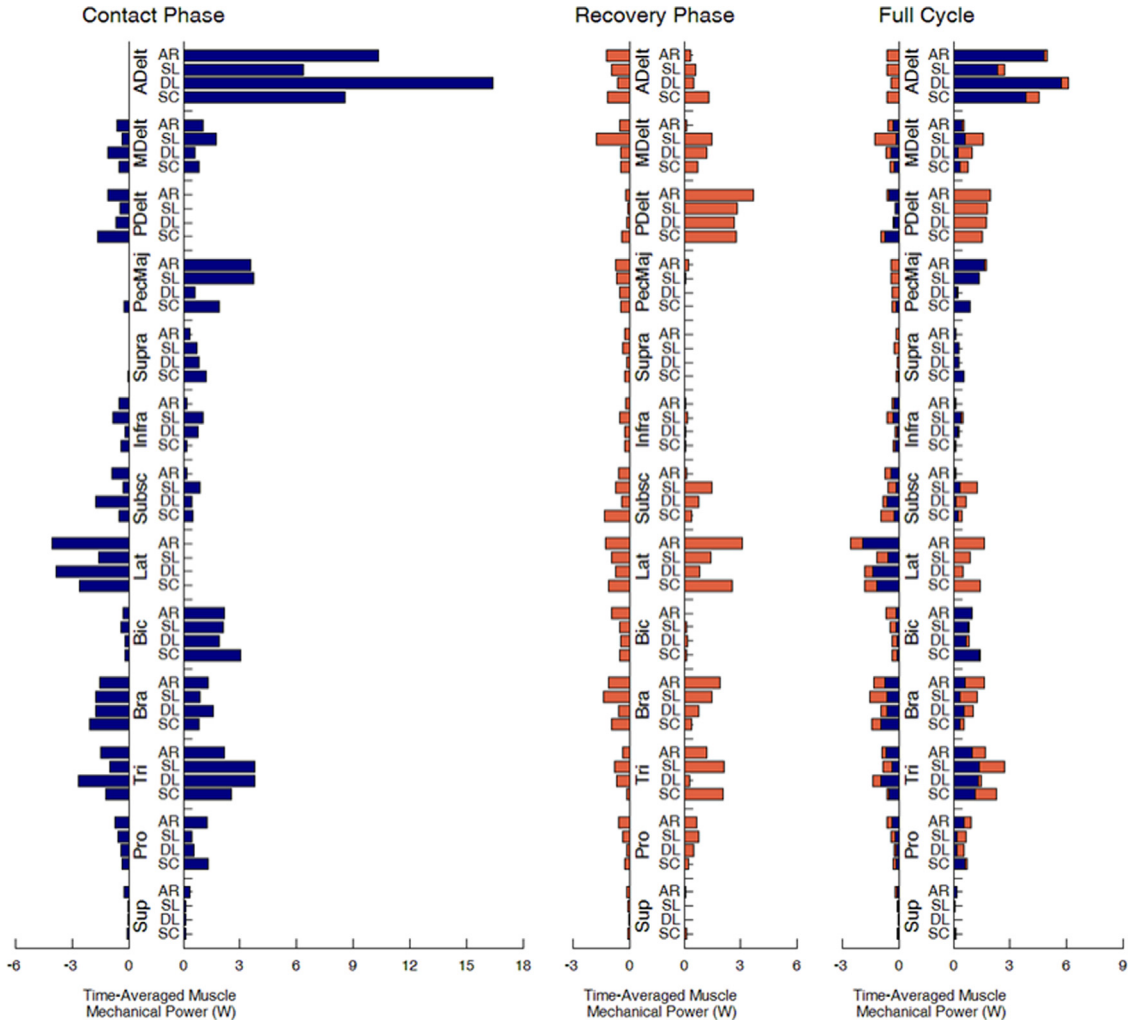

Fig. 3. Time-averaged positive and negative power generated by each muscle group for the four hand pattern types: arc (*AR*), single loop (*SL*), double loop (*DL*) and semicircular (*SC*). The left, center and right plots correspond to the contact phase, recovery phase and full cycle, respectively. Contact and recovery-phase contributions are indicated with darker (blue) and lighter (orange) shading, respectively.

experienced high contact-phase Pro stress. However, *SL* experienced low full-cycle ADelt stress, primarily due to low stress during the contact phase. *SL* also experienced low full-cycle PDelt stress due to low stresses during both phases. In addition, *SL* experienced low contact-phase Lat stress. *DL* experienced high contact-phase ADelt and Lat stresses, but low full-cycle MDelt stress, primarily due to low stress during the contact phase. *DL* also experienced low full-cycle Sup stress (due to low stress during both phases), low contact-phase PecMaj stress and low recovery-phase Lat stress. *SC* only experienced high recovery-phase Sup stress.

4. Discussion

The purpose of this study was to identify the influence of wheelchair propulsion hand pattern on upper extremity muscle demand by developing forward dynamics simulations of the four distinct hand pattern types. Contrary to our expectation that the *SC* simulation would have the lowest muscle demand, the *DL* simulation exhibited lower overall levels of demand. However, the *SC* simulation typically had the second lowest levels, and the demand was more evenly distributed throughout the full cycle, as the *DL* simulation had a shorter and more demanding contact phase. In addition to these key findings, other potential differences between the four pattern types were identified in the propulsion characteristics and muscle demand measures. While the range of full-cycle total power values only spanned 4.0 W (26.5 W for *AR* vs. 22.5 W for *DL*), this represented a 16.5% difference between patterns. Furthermore, the range of full-cycle overall muscle stress values spanned 11.5 kPa (43.0 kPa for *AR* vs. 31.5 kPa for *DL*), which is a 30.9% difference. Since manual wheelchair users can generate thousands of propulsion cycles per day (e.g., Tolerico et al., 2007), the differences in these demand levels will likely accumulate over time, and thus optimizing propulsion technique to minimize the upper extremity demand will likely reduce the risk of upper extremity pain and injury (e.g., PVACSCM, 2005).

4.1. Propulsion characteristics

While the subjects were chosen such that the four hand pattern subgroups would have similar propulsion speeds (Table 1), there were differences in other propulsion characteristics that influenced the individual muscle power and stress quantities. *SC* had a long cycle time, large contact percentage and large contact angle (Table 1), which have all previously been suggested as favorable characteristics (e.g., PVACSCM, 2005). *DL* had a long cycle time and large contact angle, but a small contact percentage. *AR* had a large contact percentage, but a short cycle time and small contact angle. *SL* had a short cycle time, small contact percentage and small contact angle, which have all been suggested as unfavorable

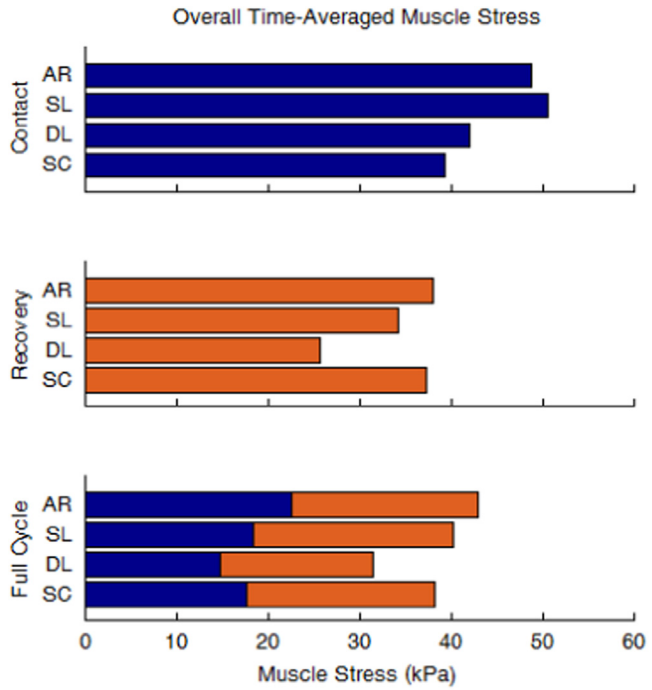

Fig. 4. Overall levels of time-averaged muscle stress (averaged across all muscles) for the four hand pattern types: arc (*AR*), single loop (*SL*), double loop (*DL*) and semicircular (*SC*). The top, middle and bottom rows correspond to the contact phase, recovery phase and full cycle, respectively. Contact and recovery-phase contributions are indicated with darker (blue) and lighter (orange) shading, respectively.

characteristics. The relative levels of these spatiotemporal variables across hand pattern types were consistent with previous studies (Boninger et al., 2002; Kwarciak et al., 2012), providing confirmation that the selected subjects appropriately represented the different hand pattern types.

4.2. Arc pattern

Of the four hand pattern types, *AR* experienced the highest levels of overall upper extremity demand across the full cycle (i.e., total muscle power and muscle stress). This was primarily due to *AR* having the highest contributions during the contact phase, derived from both high contact-phase demand levels and a large contact percentage. However, *AR* did have the lowest full-cycle Subsc stress, which may reduce the risk of fatigue and injury in this rotator cuff muscle. As Subsc plays a critical role in stabilizing the shoulder (e.g., Ward et al., 2006), this may also prevent more extensive injuries. Although the most common location for a rotator cuff tear is within Supra (e.g., Akbar et al., 2010), a Supra tear and the resulting shift of demand to the other rotator cuff muscles often leads to tears in Infra and Subsc, all of which reduces the stability of the shoulder joint and greatly increases the risk of impingement in manual wheelchair users (van Drongelen et al., 2013).

4.3. Single loop pattern

SL experienced the second highest levels of overall upper extremity demand across the full cycle. *SL* had the highest recovery-phase contributions to the total power, but lowest contact-phase contributions, leading to the second highest full-cycle average total power. *SL* also experienced the highest contact-phase stress. However, due to its small contact percentage, it experienced only the second highest contact-phase contribution to full-cycle stress which resulted in the second highest overall full-cycle stress. *SL* also experienced high Infra and Subsc stress, which could increase the risk of fatigue and injury in these rotator cuff muscles. As Infra and Subsc help stabilize the shoulder (e.g., Ward et al., 2006), this could lead to more extensive injuries (e.g., rotator cuff tears and impingement).

4.4. Double loop pattern

Of the four hand pattern types, *DL* experienced the lowest levels of overall upper extremity demand across the full cycle. This was primarily due to a combination of the lowest recovery-phase demand levels and the smallest contact percentage. Despite high demand levels during the contact phase (including the highest contact-phase total power), time spent in this phase was relatively short, and as a result *DL* actually experienced the lowest contact-phase contribution to the full-cycle average muscle stress and only the second highest contact-phase contribution to the full-cycle power. While DL has greater ranges of motion during the recovery phase, it also has the longest recovery time (Table 1), allowing this greater motion to occur over a longer period of time. This also allows a prolonged and more gradual transition between propulsive and recovery tasks, thus reducing instantaneous muscle demand levels. The low recovery-phase demand levels for *DL* were consistent with previous work suggesting that using a low cadence technique could reduce muscle power requirements during the recovery phase (Rankin et al., 2012). One potential disadvantage of the *DL* technique is that it showed increased contact-phase ADelt power combined with decreased contact-phase PecMaj power, which could increase the risk of impingement (e.g., Burnham et al., 1993; Sharkey and Marder, 1995).

4.5. Semicircular pattern

SC experienced the second lowest levels of overall upper extremity demand across the full cycle. *SC* consistently had the second lowest total power, for each individual phase and the full cycle. In addition, *SC* experienced the lowest contact-phase stress, but the second-highest recovery-phase stress. This led to the smallest percent difference between contact and recovery-phase stresses among the four hand pattern types, suggesting that upper extremity demand is most evenly distributed throughout the cycle when using *SC*. There were no individual muscles that appeared to be at a greater risk of injury during *SC* in comparison to the other hand pattern types.

4.6. Study limitations

A potential limitation of this study is that the experimental data were not collected overground but on a calibrated wheelchair ergometer. Ergometers and other stationary propulsion simulators do not perfectly replicate overground propulsion. However, they result in similar propulsion mechanics while providing greater control over experimental variables in a laboratory setting (Koontz et al., 2012).

In addition, the musculoskeletal model did not include the ability of the hand to produce a pure moment at the handrim because it did not include the wrist muscles and the wrist joint was fixed in the anatomical position. However, relative to shoulder and elbow moments, wrist moments are generally small (e.g., Robertson et al., 1996; Sabick et al., 2004). In addition, the influence of the fixed wrist on the other joints and study conclusions was minimized by using a consistent model across all simulations and requiring the optimized simulations to emulate the experimental joint kinematics and handrim forces.

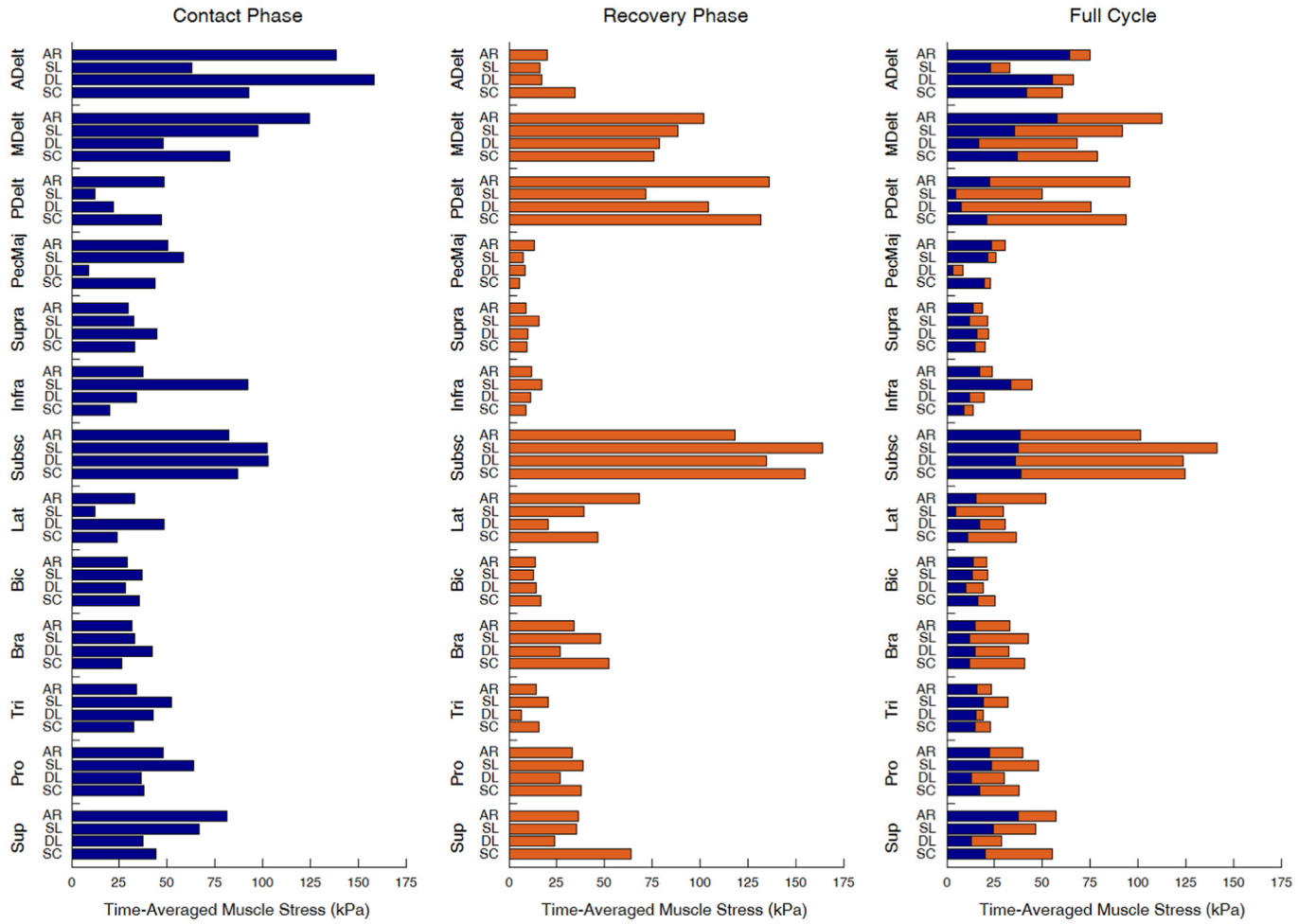

Fig. 5. Time-averaged individual muscle stress values for the four hand pattern types: arc (*AR*), single loop (*SL*), double loop (*DL*) and semicircular (*SC*). The left, center and right plots correspond to the contact phase, recovery phase and full cycle, respectively. Contact and recovery-phase contributions are indicated with darker (blue) and lighter (orange) shading, respectively.

Another potential limitation of this study is that it only examined level propulsion at a self-selected speed. Results of previous investigations suggest that people who use manual wheelchairs modify their hand pattern with changes in propulsion speed (Boninger et al., 2002; Slowik et al., 2015) and grade of incline (Richter et al., 2007; Slowik et al., 2015). Thus, future work should examine upper extremity demand during these other propulsion conditions.

Finally, only a single representative simulation was developed for each hand pattern type. This allowed the use of a computationally-intensive forward dynamics framework that included the time-dependent physiological nature of muscles, but as a result we were unable to assess the statistical significance of our identified differences. Furthermore, due to the scarcity of longitudinal studies of manual wheelchair propulsion, a threshold for clinical significance of demand levels is not yet well-defined. While these limitations should be considered when interpreting the study results, the clear differences between hand patterns support previous experimental findings that the double loop or semicircular patterns are preferred to minimize upper extremity demand and potentially prevent pain and injuries during manual wheelchair propulsion.

4.7. Summary

DL and *SC* produced the most favorable levels of upper extremity demand. While *DL* had the lowest full-cycle and recovery-phase demand values, it did require high levels of muscle power during its relatively short contact phase. The full-cycle demand levels of *SC* were the second-lowest, and the demand was more evenly distributed between the contact and recovery phases. These results suggest that when propelling their wheelchairs at a self-selected speed on level ground, individuals may want to consider using either the *DL* or *SC* pattern.

Conflict of interest statement

The authors have no conflict of interest to declare.

Acknowledgments

This study was supported by NIH Grant R01 HD049774 and a National Science Foundation Graduate Research Fellowship under Grant DGE-1110007.

References

Akbar, M., Balean, G., Brunner, M., Seyler, T.M., Bruckner, T., Munzinger, J., Grieser, T., Gerner, H.J., Loew, M., 2010. Prevalence of rotator cuff tear in paraplegic patients compared with controls. J. Bone Jt. Surg. 92, 23–30.

Boninger, M.L., Souza, A.L., Cooper, R.A., Fitzgerald, S.G., Koontz, A.M., Fay, B.T., 2002. Propulsion patterns and pushrim biomechanics in manual wheelchair propulsion. Arch. Phys. Med. Rehabil. 83, 718–723.
Burnham, R.S., May, L., Nelson, E., Steadward, R., Reid, D.C., 1993. Shoulder pain in wheelchair athletes. The role of muscle imbalance. Am. J. Sports Med. 21, 238–242.
Davy, D.T., Audu, M.L., 1987. A dynamic optimization technique for predicting muscle forces in the swing phase of gait. J. Biomech. 20, 187–201.
de Groot, J.H., Brand, R., 2001. A three-dimensional regression model of the shoulder rhythm. Clin. Biomech. 16, 735–743.
de Groot, S., Veeger, H.E., Hollander, A.P., van der Woude, L.H., 2004. Effect of wheelchair stroke pattern on mechanical efficiency. Am. J. Phys. Med. Rehabil. 83, 640–649.
Erdemir, A., McLean, S., Herzog, W., van den Bogert, A.J., 2007. Model-based estimation of muscle forces exerted during movements. Clin. Biomech. 22, 131–154.
Goffe, W.L., Ferrier, G.D., Rogers, J., 1994. Global optimization of statistical functions with simulated annealing. J. Econom. 60, 65–99.
Hall, A.L., Peterson, C.L., Kautz, S.A., Neptune, R.R., 2011. Relationships between muscle contributions to walking subtasks and functional walking status in persons with post-stroke hemiparesis. Clin. Biomech. 26, 509–515.
Happee, R., van der Helm, F.C., 1995. The control of shoulder muscles during goal directed movements, an inverse dynamic analysis. J. Biomech. 28, 1179–1191.
Holzbaur, K.R., Murray, W.M., Delp, S.L., 2005. A model of the upper extremity for simulating musculoskeletal surgery and analyzing neuromuscular control. Ann. Biomed. Eng. 33, 829–840.
Koontz, A.M., Worobey, L.A., Rice, I.M., Collinger, J.L., Boninger, M.L., 2012. Comparison between overground and dynamometer manual wheelchair propulsion. J. Appl. Biomech. 28, 412–419.
Kwarciak, A.M., Sisto, S.A., Yarossi, M., Price, R., Komaroff, E., Boninger, M.L., 2009. Redefining the manual wheelchair stroke cycle: identification and impact of nonpropulsive pushrim contact. Arch. Phys. Med. Rehabil. 90, 20–26.
Kwarciak, A.M., Turner, J.T., Guo, L., Richter, W.M., 2012. The effects of four different stroke patterns on manual wheelchair propulsion and upper limb muscle strain. Disabil. Rehabil.: Assist. Technol. 7, 459–463.
Lighthall-Haubert, L., Requejo, P.S., Mulroy, S.J., Newsam, C.J., Bontrager, E., Gronley, J.K., Perry, J., 2009. Comparison of shoulder muscle electromyographic activity during standard manual wheelchair and push-rim activated power assisted wheelchair propulsion in persons with complete tetraplegia. Arch. Phys. Med. Rehabil. 90, 1904–1915.
Mulroy, S.J., Hatchett, P., Eberly, V.J., Haubert, L.L., Conners, S., Requejo, P.S., 2015. Shoulder strength and physical activity predictors of shoulder pain in people with paraplegia from spinal injury: prospective cohort study. Phys. Ther. 95, 1027–1038.
Neptune, R.R., Kautz, S.A., Zajac, F.E., 2001. Contributions of the individual ankle plantar flexors to support, forward progression and swing initiation during walking. J. Biomech. 34, 1387–1398.
Paralyzed Veterans of America Consortium for Spinal Cord Medicine, 2005. Preservation of upper limb function following spinal cord injury: a clinical practice guideline for health-care professionals. J. Spinal Cord. Med. 28, 434–470.
Qi, L., Wakeling, J., Grange, S., Ferguson-Pell, M., 2014. Patterns of shoulder muscle coordination vary between wheelchair propulsion techniques. IEEE Trans. Neural Syst. Rehabil. Eng. 22, 559–566.
Raasch, C.C., Zajac, F.E., Ma, B., Levine, W.S., 1997. Muscle coordination of maximum-speed pedaling. J. Biomech. 30, 595–602.
Rankin, J.W., Kwarciak, A.M., Mark Richter, W., Neptune, R.R., 2010. The influence of altering push force effectiveness on upper extremity demand during wheelchair propulsion. J. Biomech. 43, 2771–2779.
Rankin, J.W., Kwarciak, A.M., Richter, W.M., Neptune, R.R., 2012. The influence of wheelchair propulsion technique on upper extremity muscle demand: A simulation study. Clin. Biomech. 27, 879–886.
Rankin, J.W., Neptune, R.R., 2012. Musculotendon lengths and moment arms for a three-dimensional upper-extremity model. J. Biomech. 45, 1739–1744.
Rankin, J.W., Richter, W.M., Neptune, R.R., 2011. Individual muscle contributions to push and recovery subtasks during wheelchair propulsion. J. Biomech. 44, 1246–1252.
Rao, S.S., Bontrager, E.L., Gronley, J.K., Newsam, C.J., Perry, J., 1996. Three-dimensional kinematics of wheelchair propulsion. IEEE Trans. Rehabil. Eng. 4, 152–160.
Richter, W.M., Rodriguez, R., Woods, K.R., Axelson, P.W., 2007. Stroke pattern and handrim biomechanics for level and uphill wheelchair propulsion at self-selected speeds. Arch. Phys. Med. Rehabil. 88, 81–87.
Robertson, R.N., Boninger, M.L., Cooper, R.A., Shimada, S.D., 1996. Pushrim forces and joint kinetics during wheelchair propulsion. Arch. Phys. Med. Rehabil. 77, 856–864.
Sabick, M.B., Kotajarvi, B.R., An, K.N., 2004. A new method to quantify demand on the upper extremity during manual wheelchair propulsion. Arch. Phys. Med. Rehabil. 85, 1151–1159.
Sharkey, N.A., Marder, R.A., 1995. The rotator cuff opposes superior translation of the humeral head. Am. J. Sports Med. 23, 270–275.
Shimada, S.D., Robertson, R.N., Boninger, M.L., Cooper, R.A., 1998. Kinematic characterization of wheelchair propulsion. J. Rehabil. Res. Dev. 35, 210–218.
Slowik, J.S., Neptune, R.R., 2013. A theoretical analysis of the influence of wheelchair seat position on upper extremity demand. Clin. Biomech. 28, 378–385.
Slowik, J.S., Requejo, P.S., Mulroy, S.J., Neptune, R.R., 2015. The influence of speed and grade on wheelchair propulsion hand pattern. Clin. Biomech.
Soltau, S.L., Slowik, J.S., Requejo, P.S., Mulroy, S.J., Neptune, R.R., 2015. An investigation of bilateral symmetry during manual wheelchair propulsion. Front. Bioeng. Biotechnol. 3, 86.
Tolerico, M.L., Ding, D., Cooper, R.A., Spaeth, D.M., Fitzgerald, S.G., Cooper, R., Kelleher, A., Boninger, M.L., 2007. Assessing mobility characteristics and activity levels of manual wheelchair users. J. Rehabil. Res. Dev. 44, 561–571.
van Drongelen, S., Schlussel, M., Arnet, U., Veeger, D., 2013. The influence of simulated rotator cuff tears on the risk for impingement in handbike and handrim wheelchair propulsion. Clin. Biomech. 28, 495–501.
Ward, S.R., Hentzen, E.R., Smallwood, L.H., Eastlack, R.K., Burns, K.A., Fithian, D.C., Friden, J., Lieber, R.L., 2006. Rotator cuff muscle architecture: implications for glenohumeral stability. Clin. Orthop. Relat. Res. 448, 157–163.
Winters, J.M., Stark, L., 1988. Estimated mechanical properties of synergistic muscles involved in movements of a variety of human joints. J. Biomech. 21, 1027–1041.